DFT insights on the $Be_{1-x}Cr_xS$ alloys for optoelectronic and magnetic devices

N. Kanwal[a], M. Ishfaq[a], S. A. Aldaghfag[b]. S. Saleem[a], M. Yaseen[a,*]
[a]*Spin-Optoelectronics and Ferro-Thermoelectric (SOFT) Materials and Devices Laboratory*, *Department of Physics, University of Agriculture Faisalabad, Faisalabad 38040, Pakistan*
[b]*Department of Physics, College of Sciences, Princess Nourah bint Abdulrahman University, P. O. Box 84428, Riyadh 11671, Saudi Arabia*

In this work, the electro-optical and magnetic characteristics of $Be_{1-x}Cr_xS$ (x= 6.25%, 12.5% and 25%) are brought into investigation by employing full potential linearized augmented plane wave (FP-LAPW) scheme designed within density functional theory (DFT). The stability of the $Be_{1-x}Cr_xS$ alloy is justified by the negative values of formation energy. The band structures and density of states are examined by using GGA functional. $Be_{1-x}Cr_xS$ compound demonstrates the half-metallic (HM) ferromagnetic behavior for all doping concentrations; spin-up channel reveals the metallic character and other spin version displays the semiconductor (SC) behavior. The values of total magnetic moment (μ_B) are recorded as 4.0 8.0 and 16.0 μ_B for corresponding 6.25%, 12.5% and 25%, which mainly arises owing to Cr-3*d* state. Moreover, optical features including dielectric function $\varepsilon(\omega)$, reflectivity, refraction, and absorption are explored within range of 0-10 eV. The maximum absorption of incident photons was found in ultraviolet (UV) span which implies their importance for optoelectronic applications. Results reveal that the studied alloy has potential applications in magnetic and optoelectronic gadgets.

(Received September 26, 2023; Accepted January 9, 2024)

Keywords: Half metallic ferromagnetism, Dilute magnetic Semiconductors, FP-LAPW, Optoelectronic applications

1. Introduction

The occurrence of magnetic ordering in condensed matter is dependent on the existence of magnetic moments and their interactions. The partially filled d-shells of transition metals (TMs) are the major reason to stabilize the magnetic ordering in solids at room temperature. Naturally occurring magnets have metallic band structures which hinders their potential usage in advanced spintronic devices. Significant efforts have been made to engineer the magnetism in semiconducting (SC) solids [1]. Over the past few years, the half-metallic ferromagnetic (HMF) and dilute magnetic semiconductor (DMS) materials have been studied extensively owing to their inimitable physical features and technological applications in the field of photovoltaic, magnetic storage and optical gadgets [1-3]. The remarkable features and functionalities of these magnets arise from their strong spin-polarization. DMS compounds (II-VI, III-V, and IV-VI) are obtained through the substitution of TMs [4] which alters the energy band gap (E_g) of host material. In addition, 3*d* transition metals (TMs) tend to exhibit higher solubility in II-VI compounds as compared to III-V SC compounds [5, 6]. These materials exhibit robust ferromagnetism at elevated temperature [1, 2] and are utilized by charge carriers in SC to produce HMF materials. Half metallic ferromagnetic material exhibits metallicity in one spin version and have a band gap (E_g) in another spin version, which yields 100% SP above the Fermi level (E_F). Owing to this exceptional behavior, the materials properties exhibited at macroscopic and nano scales offer valuable insights for achieving novel functionalities in devices.

* Corresponding author: myaseen_taha@yahoo.com
https://doi.org/10.15251/CL.2024.211.53

The II-VI semiconductors have aroused much enthusiasm in the scientific community due to their large E_g and maximum light emitting efficiency at room temperature [7-13] which make them appropriate candidates in optical gadgets e.g., blue laser, optical waveguides, spin valves and LEDs. Specifically, BeX (X= S, Se, Te) have large indirect band gaps [14-18] and crystallize into four-fold coordinate zinc blend phase under low pressure [19-22]. The bulk modulus, E_g and Philips iconicity values of these alloys increase from BeTe to BeS [23, 24] which makes them more stable materials. Also, it is found that robust covalent bonding and their small ionic radii are the distinctive characteristics that set them apart from other chalcogenide compounds. The lattice parameters of BeTe and BeS are almost similar to the gallium arsenide and zinc selenide, respectively [25]. Various theoretical studies were carried out to investigate the physical features of TM (TM= Mn, Ti, V and Cr) doped BeS alloys [26-29], while experimental work on these alloys is limited [30]. Nazir *et al*. investigated the magnetic and electronic properties of chromium (25%) -doped CdS/ZnS reporting the HMF behavior [31]. The stability of the ferromagnetic (FM) phase in chromium-doped II-VI compounds were probed through theoretical computations that rely on tight binding approximation [32]. The *p-d* exchange interaction has been observed to exhibit FM behavior while the FM character of *d-d* super-exchange still needs experimental verification for Cr-based II-VI semiconductors [33]. Using DFT, Mokaddem *et al*. examined the HMF behavior of Cr doped BeS and was regarded as a promising material for spintronic devices. The outcomes illustrated that the robust hybridization among S-3*p* and Cr-3d_{t2g} states dominated the E_g for spin-up channel and stabilized the FM ground state via double exchange mechanism [34]. HMF behavior was also observed for Cr doped BaSe by Bahloul *et al.,* and it was reported that *p-d* exchange coupling offers antiferromagnetic (AFM) feature at 75% doping and FM behavior for other concentrations [35].

Herein, first principles calculations are executed to calculate the electro-magnetic and optical characteristics of Cr-doped BeS alloy at different Cr concentrations. The analysis of the outcomes shows that the resultant compound demonstrates HMF behavior and is highly recommended for applications in spintronics and other optical gadgets.

2. Computational details

DFT is a reliable theoretical approach that has been extensively employed to investigate the physical features of solid-state systems. The FP-LAPW approach is used to calculate the physical features of the $Be_{1-x}Cr_xS$ alloys. In WIEN2k code, the Kohn-Sham equation of DFT is solved by using FP-LAPW scheme [36]. Within muffin tin (MT) sphere, the basis set is obtained by partitioning the crystal system into non-overlapping spheres which enclose each individual atom and forming an interstitial region between them. The exchange and correlation energies are taken into account by applying the generalized gradient approximation (GGA) with the Perdew-Burke-Ernzerhof (PBE) exchange-correlation potential. The charge density and potential are expended using a combination of spherical harmonics and plane waves as the basic function for the interstitial composition [38, 39]. For SCF calculations, a matrix of 10 × 10 × 10 K-mesh was employed within first Brillion zone (BZ). Electronic configurations: [He] $2s^2$ for Be, [Ne] $3s^2$ $3p^4$ for S and [Ar] $3d^5$ $4s^1$ for Cr were used in calculations. The cut-off parameter (which controls the basis set size) $R_{MT} \times K_{max}$ are selected as 8 and G_{max} = 12. The R_{MT} is the MT radius and K_{max} is the highest length of the plane wave vector. The MT radiii are taken as 2.50, 2.20, and 2.30 bohr for Cr, Be and S atoms, correspondingly. Atomic wave functions are augmented up to l_{max} = 10 to classify the spherical harmonics for ground state energy computations. For total energy convergence, the self-consistency was assumed of less than 10^{-6} Ry.

3. Results and discussions

3.1. Electronic features

The electronic characteristics including band structures (BS) and density of states (DOS) of a material are examined by the participation of various electronic states in the valance to

conduction band (VB and CB). The BS provides information about the material's nature with respect to electrical conductivity and is linked with optoelectronic characteristics [40]. The impact of magnetic (Cr) impurity on BeS compound is depicted in Fig. 1 in the form of iso-surface spin density visualization.

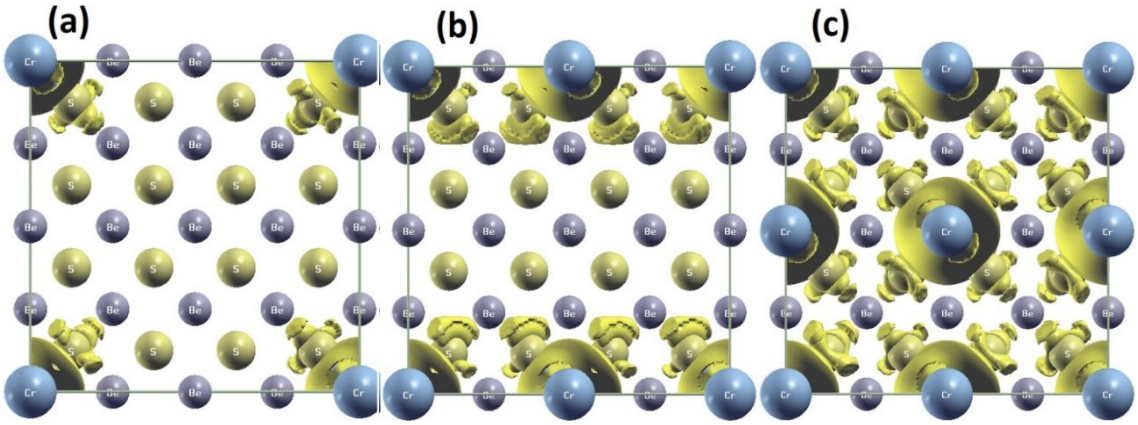

Fig. 1. Geometric illustration along with iso-surface spin density visualization for (a) $Be_{0.9375}Cr_{0.0625}S$ (b) $Be_{0.875}Cr_{0.125}S$ and (c) $Be_{0.75}Cr_{0.25}S$.

This magnetic character can be confirmed by highly asymmetric spin polarized of BS of the studied material. The plots of BS along the high symmetry direction of the first BZ of $Be_{0.9375}Cr_{0.0625}S$, $Be_{0.875}Cr_{0.125}S$, and $Be_{0.75}Cr_{0.25}S$ compounds are shown in corresponding middle panels of Figs. 2, 3 and 4. $Be_{1-x}Cr_xS$ compound reveals the HMF behavior because of the metallic nature observed in spin-up version and semiconductor (SC) character with a direct E_g in spin-down channel (see middle panels of Fig. 2-4).

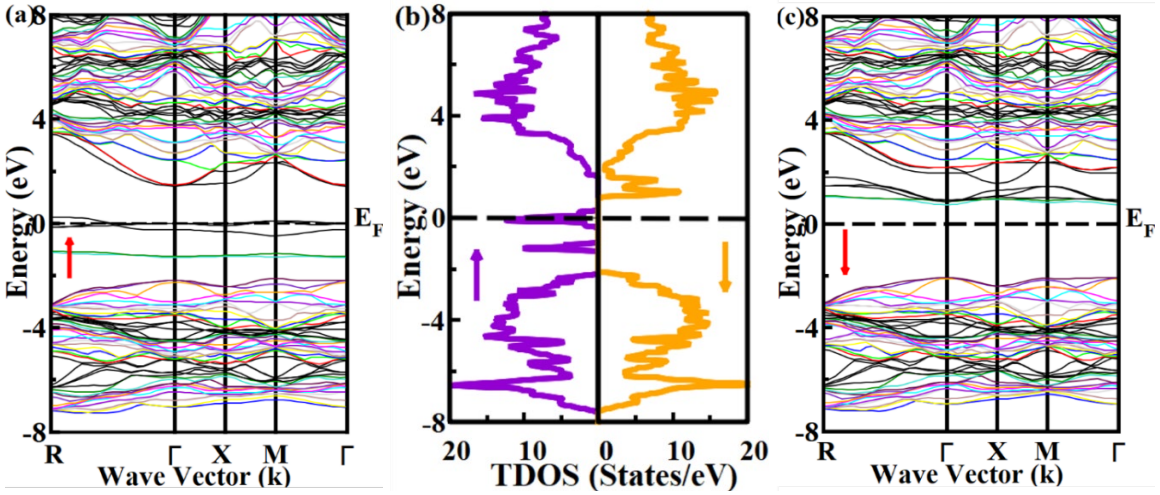

Fig. 2. Plots of BS ((a) left and (c) right) and TDOS ((b) central) of $Be_{0.9375}Cr_{0.0625}S$.

The computed values of E_g (at Γ symmetry points) in spin-down channel for $Be_{1-x}Cr_xS$ (x=6.25%, 12.5%, 25%) are 2.74, 2.84 and 2.85 eV, respectively. The electron exchange in both spin channels illustrates the ferromagnetic (FM) ordering with 100% SP. For comparison, the pristine BeS compound elucidated the SC character with E_g of 2.9 eV and owns symmetric DOS revealing zero net μ_B in previously published theoretical data [41]. This reveals the significant impact the Cr impurity causes on the electronic structure of pristine BeS.

To validate the nature and origin of ferromagnetism, the DOS are calculated for $Be_{1-x}Cr_xS$ within range of -6 to 6 eV as depicted in middle panel of Fig. 2-4 and Fig. 5(a-c). Total (T) DOS represent the number of diverse electron states available at specific energy levels and its plots exhibit good agreement with BS results [42]. The highest peaks of TDOS show the maximum participation of Cr and S atoms in VB and CB. While PDOS plots offer insights into the participation of individual atoms to specific energy levels. The participation of the Cr-*d* state is significant with minor contribution of Be-*s* and S-*p* states above Fermi level in majority spin version, which plays an important role to provoke HMF behavior in studied alloys.

For all concentrations, the VB is mainly dominated by Cr-3*d* and *p* orbitals of sulfur atom via minimum contribution of Be-*s* and S-*s* states while in CB, the peaks arises owing to the Cr-3*d* state with an admixture of *s*-state of beryllium and *p*-states of sulfur atom in both spins (up and down) versions (see Fig. 5a-c). There exists a strong hybridization owing to *d*-orbit of chromium *p* orbit of sulfur atoms across the Fermi level in majority spin version. Thus, the computed features indicate that the resultant compound has prospective applications in spintronic and optical devices.

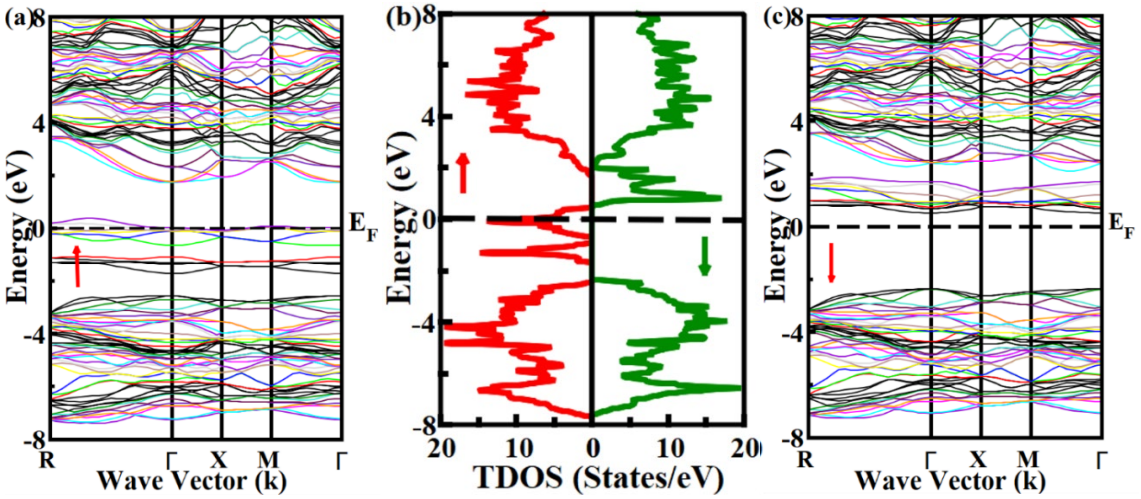

Fig. 3. Plots of BS ((a) left and (c) right) and TDOS ((b) central) of $Be_{0.875}Cr_{0.125}S$.

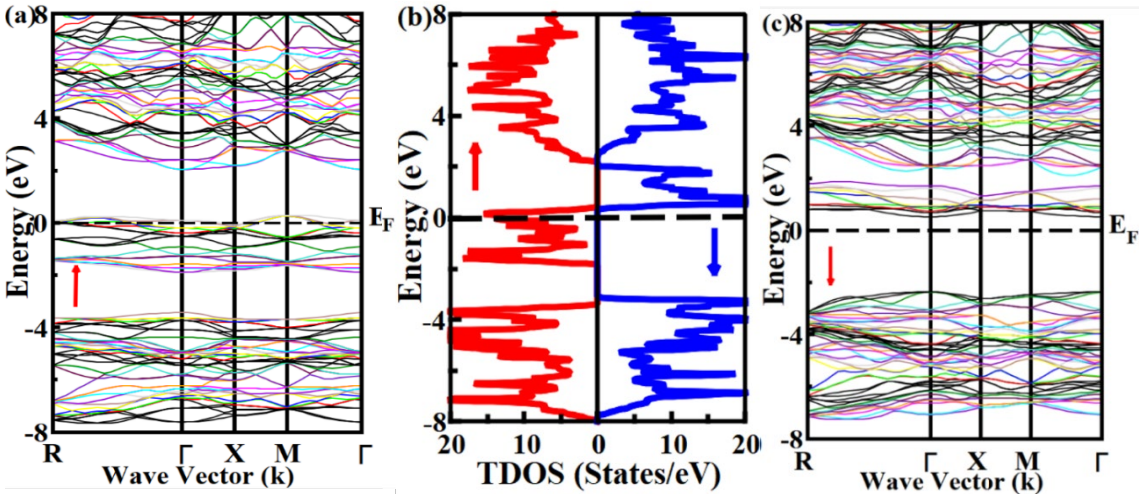

Fig. 4. Plots of BS ((a) left and (c) right) and TDOS ((b) central) of $Be_{0.75}Cr_{0.25}S$.

To examine the material's thermodynamical stability, the formation energy (ΔE_f) is computed by the following formula [43] and illustrated in Table 1.

$$\Delta Ef = E_{Total}(Be_{1-x}Cr_xS) - lE_{Be} - mE_{Cr} - nE_S \quad (1)$$

Here, $E_{Total}(Be_{1-x}Cr_xS)$ denotes the overall energy of the resultant compound and *l*, *m*, *n* signifies the number of atoms per unit cell. E_{Be}, E_{Cr} and E_S represent the energies of the individual components in their respective bulk form at the ground state. Table 1 depicts the negative ΔE_f values for all doped systems, which corresponds to the thermodynamical stability. The positive values of ΔE_f show unstable behavior of the material while negative values provide confirmation of stability in FM phase for corresponding compounds [44].

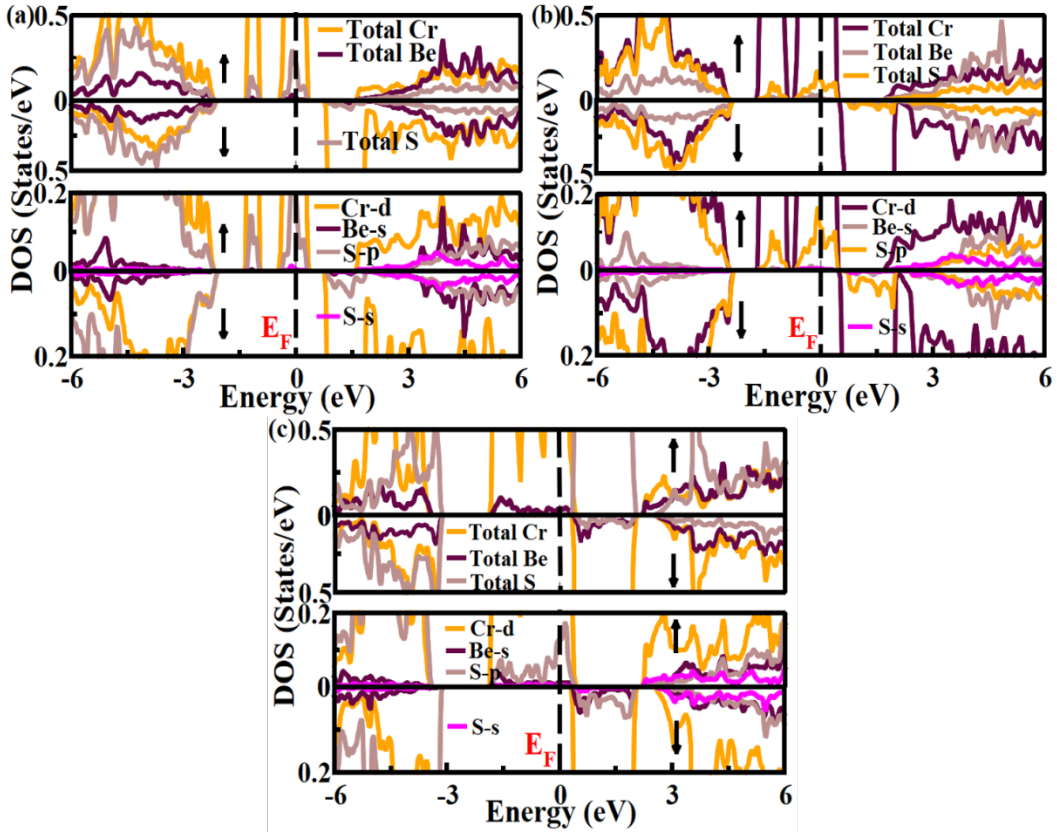

Fig. 5. Plots of SP-TDOS and PDOS of $Be_{1-x}Cr_xS$ compound at (a) $Be_{0.9375}Cr_{0.0625}S$ (b) $Be_{0.875}Cr_{0.125}S$ and (c) x= $Be_{0.75}Cr_{0.25}S$.

Table 1. Formation energies of Cr doped Bes alloy.

Concentrations of Cr %	6.25	12.5	25
Formation energy (E_F)	-2.69	-2.91	-3.12

3.2. Optical properties

In order to fabricate the optoelectronic gadgets, it is inevitable to explore the light interaction with semiconducting materials. In this way, some physical mechanisms including the interband transitions happen in the materials which is explained by the optical characteristics in terms of frequency-dependent optical parameters. Various optical parameters of $Be_{1-x}Cr_xS$ alloys are calculated within range of 0-10 eV to inspect their prospective usage in optoelectronic, solar cells and UV photodetectors gadgets. Optical parameters are calculated from dielectric function $\varepsilon(\omega)$ which can be investigated via the expression of $\varepsilon(\omega) = \varepsilon_1(\omega) + \varepsilon_2(\omega)$ [45-47]. Where $\varepsilon_1(\omega)$ represents the real part of the $\varepsilon(\omega)$ and is linked via the reflection/scattering of the system. $\varepsilon_2(\omega)$

indicates the imaginary part of ε(ω) and is directly related to absorption spectra [48]. $\varepsilon_1(\omega)$ and $\varepsilon_2(\omega)$ are related according to the Kramers-Kronig relation [49]:

$$\varepsilon_1(\omega) = 1 + \frac{2}{\pi} P \int_0^{\infty} \frac{\omega \varepsilon_2(\omega)}{\omega^2 - \omega^2} d\,\omega \tag{2}$$

$$\varepsilon_2(\omega) = \frac{e^2 \hbar}{\pi m^2 \omega^2} \sum_{vc} \int |n, n'(k, q)|^2 \, \delta\left[\omega_{n,\acute{n}}(k) - \omega\right] d^3k \tag{3}$$

At zero frequency, $\varepsilon_1(\omega)$ is reported as 25.6, 30.1, and 58.2 for 6.25%, 12.5% and 25% doping of Cr, respectively (see Table 2). Afterwards, $\varepsilon_1(\omega)$ spectral lines decline with increasing energy of incident electromagnetic (EM) wave (see Fig. 6a).

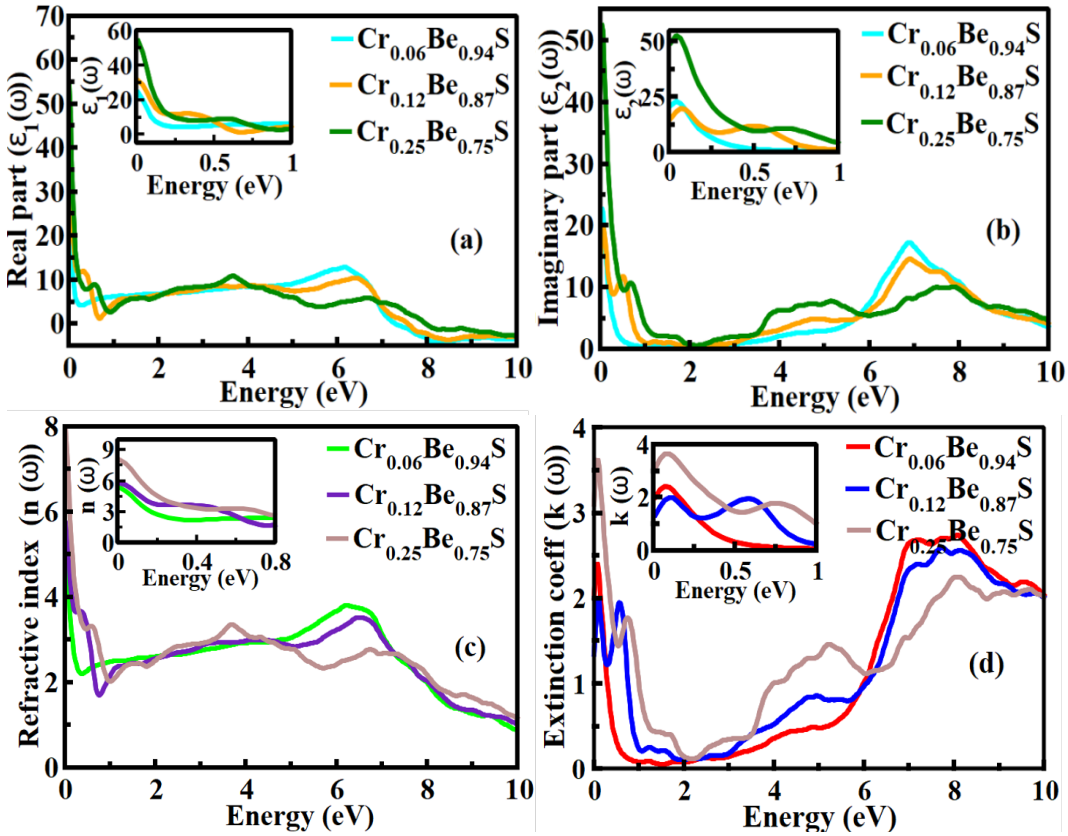

Fig. 6. Plots of (a) ε_1 (ω), (b) ε_2 (ω), (c) n (ω) and (d) k (ω) of Cr doped BeS.

Beyond the 6.72 eV energy, $\varepsilon_1(\omega)$ reaches below zero for all concentrations, exhibiting metallic nature. This metallic behavior is attributed to the excitation of substantial effective mass (collectively) which is energized by an electric field [50]. Moreover, E_g and $\varepsilon_1(0)$ of the investigated alloys also adhere to Penn's model, which can be expressed as $\varepsilon_1(0) \approx 1 + (\hbar\omega_p/E_g)^2$ [51]. The absorptive nature of the compound is proved by $\varepsilon_2(\omega)$ which corresponds to the BS. The $\varepsilon_2(\omega)$ is expressed as electronic transitions from VB to CB [52]. The threshold (critical) energy points of $\varepsilon_2(\omega)$ occur in 1.4-3.1 eV range for $Be_{1-x}Cr_xS$ alloys (see Fig. 6b). The prominent peaks can be identified at 7.4, 7.7 and 7.9 eV for corresponding 6.25%, 12.5% and 25% Cr doping. Hence, maximum absorption is exhibited in the UV spectral zone, endorsing that the studied alloy is a suitable candidate for high energy optical device applications. Path change of incident light is scrutinized by refractive index n(ω), which describes the bonding character of the substance [53]. At zero frequency, n(ω) values are 5.4, 6.2 and 8.1 for $Be_{1-x}Cr_xS$ (x= 6.25%, 12.5% and 25%), correspondingly (see Table 2). These values are greater than unity showing that photons are

slowed down as passing through materials owing to electron interactions. The n(ω) upsurges to the maximum values at 6.82 electron volt for all doping concentrations and then decays with increasing photon energy (see Fig. 6c) because photons are not directly de-excited to lower energy state, leading to energy dissipation [26]. The n(ω) is correlated with real part of the ε(ω) via relation k^2-n^2 = $\varepsilon_1(\omega)$ [54]. The extinction coefficient k(ω) signifies the reduction in the intensity of light (k > 0) as it passes through a system. It is related to $\varepsilon_2(\omega)$ through relation: 2kn = $\varepsilon_2(\omega)$. The k(ω) plays an important character in controlling the behavior of EM as passing through the system [55]. The local maxima value for k(ω) related to the zero value of real part is 2.66, 2.52 and 2.41 at 7.51, 7.74 and 8. 35 eV for $Be_{1-x}Cr_xS$ (x= 6.25%, 12.5%, 25%), respectively (see Fig. 6d).

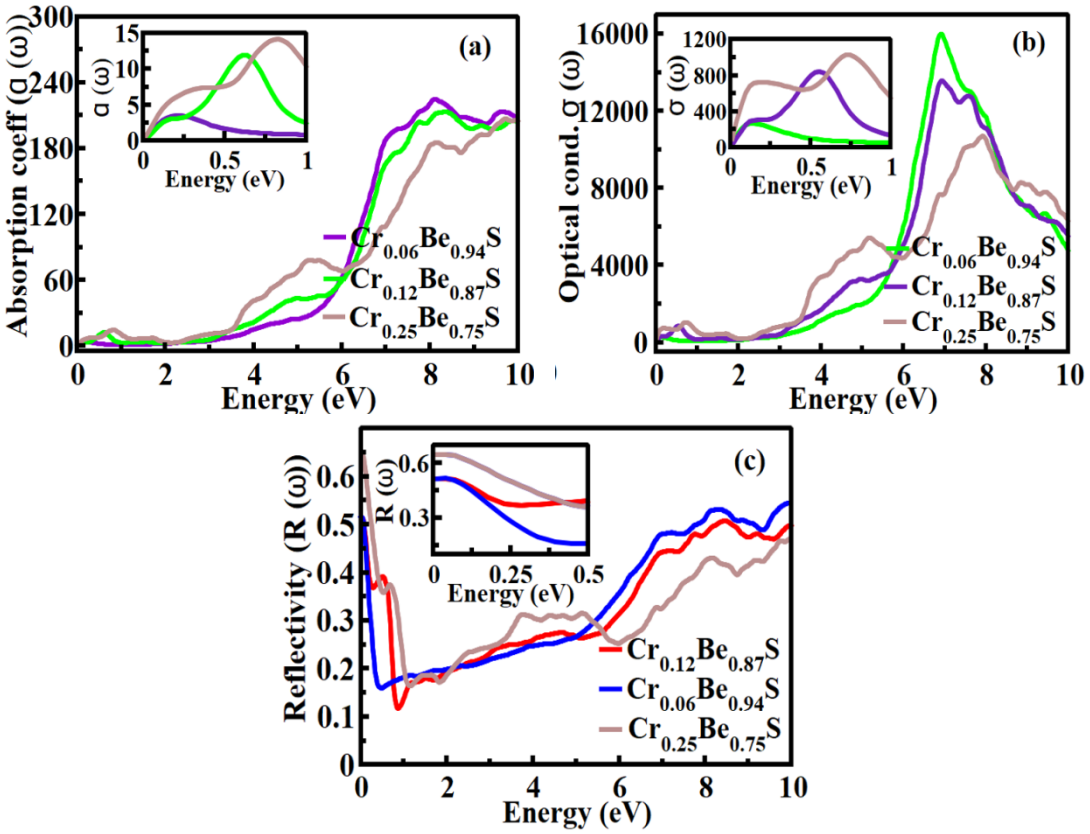

Fig. 7. Plots of (a) α (ω), (b) σ (ω) and (c) R (ω) of Cr doped BeS.

Absorption coefficient α(ω) is a vital parameter of optical characteristics and provides valuable insights into the application of electro-optical materials. The α(ω) reveals the rate of decay in energy per unit distance as EM radiation penetrates the system and also analyzes the absorptive nature of materials [56]. It can be calculated form computed k(ω) using the relation:

$$\alpha(\omega) = \frac{4\pi k}{\lambda} \tag{4}$$

The absorption edges of α(ω) are directly associated with the E_g which are 2.82, 2.71, 2.74 eV for $Be_{1-x}Cr_xS$ (x= 6.25%, 12.5% and 25%), correspondingly. After edge points, α(ω) increases via energy and reaches its maximum value around 6.8-7.9 eV (see Fig. 7a) in the UV spectral region. Uppermost peaks are displayed owing to valance to conduction band transitions while smaller curves emerge due to sub-bands [57, 58]. Peaks values of the resultant compound appeared in UV region which is similar to other related alloys such as $Be_{1-x}Mn_xTe$ (5.2-7.1 eV) [43] and $Be_{1-x}V_xSe$ (6.4-7.3 eV) [59] that revealed highest absorption in this span and suggest the material for optoelectronic applications. Another optical parameter, optical conductivity σ(ω) characterizes the

rise in conductivity of material owing to absorption's light and is dependent on inter/intra-band transitions. It also describes the process of bond-breaking as light interacts with the material's surface [60]. The σ(ω) and α(ω) plots have parallel behavior because diminution of light is correlated with an increase in electron concentration in CB [59]. σ(ω) curve starts to increase as photons of threshold frequency fall on the material's surface and attain peak values such as 1650 $(\Omega cm)^{-1}$, 1420 $(\Omega cm)^{-1}$ and 1580 $(\Omega cm)^{-1}$ at 7.74, 7.75 and 7.98 eV for $Be_{1-x}Cr_xS$ (x= 6.25%, 12.5% and 25%), correspondingly (see Fig. 7b). Its peak values reveal that $Be_{1-x}Cr_xS$ compound is a potential material in higher energy range above threshold frequency. As light interacts with the material's surface, it undergoes simultaneous processes of absorption, reflection and transmission. To examine the light that bounces off the material's surface [61], the reflection coefficient R(ω) is also computed and shown in Fig. 7c.

Table 2. Computed static optical parameters: $\varepsilon_1(0)$, n(0) and R(0) of Cr doped BeS alloys.

Compounds	E_g(eV)	$\varepsilon_1(0)$	n(0)	R(0)
$Be_{0.9375}Cr_{0.0625}S$	2.74	25.6	5.4	0.45
$Be_{0.875}Cr_{0.125}S$	2.84	30.1	6.2	0.52
$Be_{0.75}Cr_{0.25}S$	2.85	58.2	8.1	0.71

At zero electron volt, the estimated R(ω) is 0.45, 0.52 and 0.71 for 6.25%, 12.5% and 25% concentrations, correspondingly (see Table 2). The highest R(ω) is observed within range of 6.5-8.0 eV in UV zone where the $\varepsilon_1(\omega)$ show negative peak. The obtained outcomes for $\varepsilon_1(0)$, n(0) and R(0) have been listed in Table 2. Optical features reveal that the studied material is suitable for solar cells, photodetectors and optoelectronic gadgets.

3.3. Magnetic features

The partial, total and interstitial magnetic moments (μ_B) of $Be_{1-x}Cr_xS$ (x= 6.25%, 12.5% and 25%) are calculated and summarized in Table 3. SP-DFT is used to explore the magnetic characteristics of the alloy [62]. The values of the total μ_B are 4.0, 8.0 and 16.0 for 6.25%, 12.5% and 25% doping concentration, respectively. The outcome shows that the Cr and Be atoms have more participation in inducing total μ_B as compared to the S atom, additional, it is confirmed from spin-dependent magnetic density (see Fig. 1). The spin configuration of individual atom in system is represented by the positive and negative signs, indicating the spin direction of the electrons associated with that atom [63]. The positive integer values of atoms favor the parallel alignment of μ_B while opposite signs tend to exhibit an anti-parallel configuration of μ_B. Commonly, the parallel alignment of μ_B is the dominant factor contributing to an increase in the total μ_B of studied alloy.

Table 3. The individual, interstitial and total μ_B of Cr doped BeS alloy.

Concentrations	Interstitial (μ_B)	Cr (μ_B)	Be (μ_B)	S (μ_B)	Total (μ_B)
6.25%	0.91360	2.76227	0.01836	0.00237	4.00030
12.5%	1.84145	2.75999	0.03204	0.00788	8.00318
25%	3.69145	2.75802	0.06736	0.02521	16.03229

4. Conclusion

DFT calculations are done to examine the electro-magnetic and optical characteristics of the $Be_{1-x}Cr_xS$ (x = 6.25%, 12.5% and 25%) compound. The outcome of the ΔE_f confirms the stability of $Be_{1-x}Cr_xS$ alloy in the cubic phase. Cr doped BeS alloy exhibits the HMF behavior with 100% spin polarization. The analysis of the BS and DOS reveals that partially filled Cr-*d* and S-*p*

states exhibit hybridization. In addition, the HMF character is validated by the integral values of μ_B and Cr-*d* state is identified as the primary contributor to magnetization. Dielectric functions and other optical parameters are investigated to study the optical characteristics of $Be_{1-x}Cr_xS$ compound. Cutoff values of frequency dependent reflectivity are 0.45, 0.52 and 0.71 for 6.25%, 12.5% and 25% concentrations, respectively. The upper-most conductivity σ(ω) peaks are computed as 1650, 1420 and 1580 $(\Omega cm)^{-1}$ for $Be_{1-x}Cr_xS$ (x = 6.25%, 12.5% and 25%) alloy, correspondingly. Furthermore, maximum α(ω) and n(ω) in UV range enables the material potential usage for UV photodetectors, magnetic and solar absorbing devices.

Acknowledgements

The authors express their gratitude to Princess Nourah bint Abdulrahman University Researchers Supporting Project number (PNURSP2024R81), Princess Nourah bint Abdulrahman University, Riyadh , Saudi Arabia.

References

[1] B. Doumi, A. Mokaddem, L. Temimi, N. Beldjoudi, M. Elkeurti, F. Dahmane, A. Sayede, A. Tadjer, M. Ishak-Boushaki, The European Physical Journal B 88(93), 1-9 (2015); https://doi.org/10.1140/epjb/e2015-50746-9.
[2] M. Berber, B. Doumi, A. Mokaddem, Y. Mogulkoc, A. Sayede, A. Tadjer, Journal of Computational Electronics 16, 542–547 (2017); https://doi.org/10.1007/s10825-017-1038-z.
[3] F. Matsukura, Y. Tokura, H. Ohno, Nature Nanotechnology 10(3), 209–220 (2015); https://doi.org/10.1038/nnano.2015.22.
[4] A. Mokaddem, B. Doumi, A. Sayede, D. Bensaid, A. Tadjer, M. Boutaleb, Journal of Superconductivity and Novel Magnetism 28, 157-164 (2015); https://doi.org/10.1007/s10948-014-2828-1.
[5] Z.H. Yin, J.M. Zhang, Physics Letter A 380 (35), 2796–2802 (2016); https://doi.org/10.1016/j.physleta.2016.06.042.
[6] J.P. Tang, L.L. Wang, W.Z. Xiao, X.F. Li, The European Physical Journal B 86 (362), 1-5 (2013); https://doi.org/10.1140/epjb/e2013-31162-9.
[7] A.H. Reshak, I.V. Kityk, R. Khenata, S. Auluck, Journal of Alloys and Compounds 509, 6737–6750 (2011); https://doi.org/10.1016/j.jallcom.2011.03.029.
[8] Y. Saeed, S. Nazir, A. Shaukat, A.H. Reshak, Journal of Magnetism and Magnetic Materials 322(20), 3214–3222 (2010); https://doi.org/10.1016/j.jmmm.2010.06.001.
[9] T. Ouahrani, A.H. Reshak, R. Khenata, B. Amrani, M. Mebrouki, A. Otero-de-laRoza, V. Luana, Journal of Solid State Chemistry 183(1), 46–51 (2010); https://doi.org/10.1016/j.jssc.2009.09.034.
[10] Y.A. Douri, A.H. Reshak, H. Baaziz, Z. Charifi, R. Khenata, S. Ahmad, U. Hashim, Solar Energy 84 (12), 1979–1984 (2010); https://doi.org/10.1016/j.solener.2010.10.006.
[11] A.H. Reshak, S. Auluck, Physica B Condensed Matter 388(1-2), 34–42 (2007); https://doi.org/10.1016/j.physb.2006.05.003
[12] A.H. Reshak, Journal of Chemical Physics 124, 104707–104712 (2006); https://doi.org/10.1063/1.2178801
[13] R. Khenata, A. Bouhemadou, M. Sahnoun, A.H. Reshak, H. Baltache, M. Rabah, Computational Materials Science 38 (1), 29–38 (2006); https://doi.org/10.1016/j.commatsci.2006.01.013
[14] A. Waag, F. Fischer, H. J. Lugauer,T. Litz, J. Laubender, U. Lunz, U. Zehnder, W. Ossau, T. Gerhardt, M. Möller, G. Landwehr, Journal of Applied Physics **80**, 792-796 (1996); https://doi.org/10.1063/1.362888
[15] Fischer, F., Landwehr, G., Litz, T., Lugauer, H.J., Zehnder, U., Gerhard, T., Ossau, W., Waag, A. Journal of Crystal Growth **175**, 532-540 (1997); https://doi.org/10.1016/S0022-0248(97)00127-9

[16] F. E. H. Hassan, H. Akbarzadeh, Compoutattional Material Science **35** (4), 423-431 (2006); https://doi.org/10.1016/j.commatsci.2005.02.010
[17] R. Khenata, A. Bouhemadou, M. Hichour, H. Baltache, D. Rached, M. Rérat, Solid State Electronics **50** (7-8) 1382-1388 (2006); https://doi.org/10.1016/j.sse.2006.06.019
[18] D. Heciri, L. Beldi, S. Drablia, H. Meradji, N.E. Derradji, H. Belkhir, B. Bouhafs, Computational Materials Science **38 (4)**, 609-617 (2007); https://doi.org/10.1016/j.commatsci.2006.04.003
[19] A. Muñoz, P. Rodríguez-Hernández, A. Mujica, Physica Status Solidi B, Basic Solid State Phys. **198** (1), 439 (1996); https://doi.org/10.1002/pssb.2221980157
[20] W. Akbar, S. Nazir, Journal of Alloys and Compounds 743, 83-86 (2018); https://doi.org/10.1016/j.jallcom.2018.01.349
[21] S. Padmavathi, R. John, Materials Science and Engineering: B 248, 114401 (2019); https://doi.org/10.1016/j.mseb.2019.114401
[22] P. Li, C. W. Zhang, J. Lian, M. J. Ren, P. J Wang, X. H. Yu, S. Gao, Optics Communications 295, 45-52 (2013); https://doi.org/10.1016/j.optcom.2012.12.086
[23] M. Miura, H. Murata, Y. Shiro, K. lishi, Journal of Physics and Chemistry of Solids 42 (10), 931-936 (1981); https://doi.org/10.1016/0022-3697(81)90020-2
[24] B. Bouhafs, H. Aourag, M. Ferhat, M. Certier, Journal of Physics. Condensed Matter 11 (30), 5781 (1999); https://doi.10.1088/0953-8984/11/30/309
[25] O. Madelung, Semiconductor Basic Data, Springer-Verlag, New York, 1996
[26] H. Ambreen, M. Yaseen, A. Ghaffar, M. Zahid, Material Science Semiconducting. Process. 127, 105697 (2021); https://doi.org/10.1016/j.mssp.2021.105697
[27] A. Mokaddem, B. Doumi, A. Sayede, D. Bensaid, A. Tadjer, M. Boutaleb, Journal of Superconductivity and Novel Magnetism 28 (1), 157–164 (2015); https://doi.org/10.1007/s10948-014-2828-1
[28] B. Doumi, A. Tadjer, F. Dahmane, A. Djedid, A. Yakoubi, Y. Barkat, L. Hamada, Journal of Superconductivity and Novel Magnetism 27 (2), 293–300 (2014); https://doi.org/10.1007/s10948-013-2401-3
[29] H. S. Saini, A. K. Pundir, V. Mehta, N. Nisha, P. Mehra, M. K. Kashyap, AIP Conference Proceedings 2006 (1), 030019 (2018); https://doi.org/10.1063/1.5051275
[30] E. A. Albanesi, C. M. I. Okoye, C. O. Y. Rodríguez, E. P. Blanca, A. G. Petukhov, Physical Review B 61(24), 16589 (2000); https://doi.org/10.1103/PhysRevB.61.16589
[31] S. Nazir, N. Ikram, S. A. Siddiqi, Y. Saeed, A. Shaukat, A. H. Reshak, Curr. Opin. Solid State Material Science 14 (1), 1–6 (2010); https://doi.org/10.1016/j.cossms.2009.08.001
[32] J. Blinowski, P. Kacman, J. A. Majewski, Journal of Crystal Growth 159 (1-4), 159:972 (1996); https://doi.org/10.1016/0022-0248(95)00719-9
[33] M. Jouanne, J. F. Morhange, E. Dynowska, E. Luakowska, W. Szuszkiewicz, L. W. Molenkamp, G. Karczewski, Journal of Alloys and Compounds 382 (1-2), 92-99 (2004); https://doi.org/10.1016/j.jallcom.2004.05.039
[34] A. Mokaddem, B. Doumi, B, A. Sayede, D. Bensaid, A. Tadjer, M. Boutaleb, Journal of Superconductivity and Novel Magnetism 28, 157-164 (2015); https://doi.org/10.1007/s10948-014-2828-1
[35] H. Bahloul, A. Mokaddem, B. Doumi, M. Berber, A. Boudali, Journal of Superconductivity Novel Magnetism 32, 2185–92 (2019); https://doi.org/10.1007/s10948-018-4948-5
[36] M. Arshad, M. Yaseen, S. A. Aldaghfag, S. Saleem, M. Ishfaq, M. Nazar, E. Yousef, H. H. Hegazy, Chalcogenide Lett 19(8), 553-563 (2022); https://doi.org/10.15251/CL.2022.198.553
[37] M. Yaseen, H. Ambreen, M. Zia, H. A. Javed, A. Mahmood, A. Murtaza, Journal of Superconductivity and Novel Magnetism 34, 135-141 (2021); https://doi.org/10.1007/s10948-020-05674-0
[38] A. H. Reshak, M.S. Abu-Jafar, Y. Al-Douri, Journal of Applied Physics 119, 245303 (2016); https://doi.org/10.1063/1.4954293
[39] M. Ameri, F. Bennar, S. Amel, I. Ameri, Y. Al-Douri, D. Varshney, Phase Transitions 89 (12), 1236–1252 (2016); https://doi.org/10.1080/01411594.2016.1162791
[40] P. A. Nawaz, G. M. Mustafa, S. S. Iqbal, N. A. Noor, T. S. Ahmad, A. Mahmood, R. Neffati, Solar Energy 231, 586-592 (2022); https://doi.org/10.1016/j.solener.2021.11.076

[41] K. Sina, R. Rami, L.B. Drissi, N. Rkhioui, M. D. El Bouzaidi, R. A. Laamara, Computational Condensed Matter 31, e00657 (2022); https://doi.org/10.1016/j.cocom.2022.e00657
[42] M. U. Din, Q. Ain, M. Yousaf, J. Munir, Materials Science in Semiconductor Processing 152, 107081 (2022); https://doi.org/10.1016/j.mssp.2022.107081
[43] H. Ambreen, S. A. Aldaghfag, M. Yaseen, M. Zahid, H. H. Somaily, Physica Scripta, 97(4), 045702 (2022); https://doi.org/10.1088/1402-4896/ac58cd
[44] A. Kundu, S. Ghosh, R. Banerjee, S. Ghosh, B. Sanyal, Sci. Rep. 7 (1), 1–15 (2017); https://doi.org/10.1038/s41598-017-01782-5
[45] S. Touam, R. Belghit, R. Mahdjoubi, Y. Megdoud, H. Meradji, M. S. Khan, R. Ahmed, R. Khenata, S. Ghemid, D. P. Rai, Y. Al-Douri, Bulletin of Materials Science 43, 1–11 (2020); https://doi.org/10.1007/s12034-019-1978-y
[46] Y. Al-Douri, M. Ameri, A. Bouhemadou, K. M. Batoo, Physica Status Solidi Basic 256 (11), 1–4 (2019); https://doi.org/10.1002/pssb.201900131
[47] H. Absike, N. Baaalla, L. Attou, H. Labrim, B. Hartiti, H. Ez-Zahraouy, Solid State Communction 3,114684 (2022); https://doi.org/10.1016/j.ssc.2022.114684
[48] M. Rashid, A. S. Alghamdi, Q. Mahmood, M. Hassan, M. Yaseen, A. Laref, Physica Scripta 94 (12), 125709 (2019); https://doi.org/10.1088/1402-4896/ab154f
[49] G. Marius, The physics of semiconductors: Kramers-Kronig relations, 775–776 (2010); http://dx.doi.org/10.1007/978-3-642-13884-3
[50] G. Marius, Kramers-Kronig Relations (The Physics of Semiconductors), Springer, Berlin Heidelberg, 2010
[51] S. Wemple, M. DiDomenico Jr, Physical Review B 3, 1338 (1971); https://doi.org/10.1103/PhysRevB.3.1338
[52] M. Ziati, H. Ez-Zahraouy, Optik 231, 166440 (2021); https://doi.org/10.1016/j.ijleo.2021.166440
[53] S. A. Khandy, D. C. Gupta, RSC Advances 6 (53), 48009–48015 (2016); https://doi.org/10.1039/C6RA10468A
[54] I. Aguilera, P. Palacios, K. S anchez, P. Wahnon, Physical. Review B Condensed Matter 81, 1–9 (2010); https://doi.org/10.1103/PhysRevB.81.075206
[55] M. A. Khan, H. A. Alburaih, N. A. Noor, A. Dahshan, Solar Energy 225, 122-128 (2021); https://doi.org/10.1016/j.solener.2021.07.026
[56] Q. Mahmood, S. Khalil, M. Hassan, M. A. Laref, Materials Research Bulletin 107, 225-235 (2018); https://doi.org/10.1016/j.materresbull.2018.07.039
[57] A. Hossain, M. S. I. Sarker, M. K. R. Khan, M. M. Rahman, Material. Science. Engeering B Solid-State Material Advanced Technology 253, 114496 (2020); https://doi.org/10.1016/j.mseb.2020.114496
[58] Y. Huang, W. Jie, G. Zha, Journal of Alloys and Compounds 555, 117–122 (2013); https://doi.org/10.1016/j.jallcom.2012.11.201
[59] H. Ambreen, S. Saleem, S. A. Aldaghfag, S. Noreen, M. Zahid, M. Ishfaq, M. Yaseen, Physica B: Condensed Matter 667, 415156 (2023); https://doi.org/10.1016/j.physb.2023.415156
[60] M. I. Hussain, R. A. Khalil, F. Hussain, M. Imran, A. M. Rana, S. Kim, Materials Science in Semiconductor Processing 113, 105064 (2020); https://doi.org/10.1016/j.mssp.2020.105064
[61] L. Shoukat, M. K. Butt, S. Saleem, Z. M. Elqahtani, S. A. Aldaghfag, M. Ishfaq, M. Yaseen, E. Yousef, H. H. Hegazy, Journal of Ovonic Research 18(5) 649-659 (2022); https://doi.org/10.15251/JOR.2022.185.649
[62] S. Saleem, M. Yaseen, S. A. Aldaghfag, R. Neffati, Physica Scripta 97(9), 095817 (2022); https://doi.org/10.1088/1402-4896/ac8a27
[63] S. Saleem, M. Ishfaq, S.A. Aldaghfag, M. Sajid, M. Yaseen, Physica B: Condensed Matter 667, 415163 (2023); https://doi.org/10.1016/j.physb.2023.415163